JOURNAL OF MATERIALS SCIENCE 26 (1991) 2037–2044

Effect of annealing on magnetic properties and microstructure of electroless nickel–copper–phosphorus alloy deposits

KANG-HEON HUR, JAE-HAN JEONG, DONG NYUNG LEE
Department of Metallurgical Engineering, Seoul National University, Seoul 151-742, Korea

The relationship between magnetic properties and microstructure of the as-deposited and heat-treated Ni–Cu–P alloy deposits has been studied by means of vibrating sample magnetometry, differential scanning calorimetry, X-ray diffractometry and hot-stage transmission electron microscopy. The Ni–Cu–P deposits consist of low-P Ni–Cu solid solution crystallites and high-P–low-Ni–Cu amorphous phase. When the deposits are annealed at elevated temperatures, the Ni–Cu crystallites grow rejecting P from themselves and absorbing Cu from the neighbouring amorphous phase, while the P-rich amorphous phase transforms into Ni_5P_2 phase or into Ni_5P_2 and Ni_3P phases. The metastable Ni_5P_2 phase finally transforms into the stable Ni_3P phase. The non-magnetism observed in Ni–Cu–P deposits having a copper content above 28% in both as-deposited and annealed states, is attributed to their Cu-rich Ni–Cu solid solution crystallites. Nickel phosphides which crystallize from the amorphous phase existing mixed with the Ni–Cu crystallites in the as-deposited state, do not affect the saturated magnetic moment of the deposits.

1. Introduction

Electroless Ni–P alloys have been extensively studied by many authors [1–5] due to their excellent corrosion resistance, wear resistance, uniformity and non-magnetic characteristics. However, the Ni–P alloys, mostly in the amorphous phase, have rather poor stability against heating, that is, they are easily crystallized when heated, which makes the alloys lose their non-magnetic characteristics. The non-magnetic property is especially important when the alloys are used for underlayers of magnetic recording discs. Recently, electroless Ni–Cu–P deposits showing excellent non-magnetic characteristics against heating have been developed [6–8]. Most studies on the Ni–Cu–P alloys have been confined to plating process and general properties. There have been no reports on the microstructure and crystallization behaviour and associated magnetic properties of the electroless Ni–Cu–P deposits having various compositions.

The purpose of this work was to study the microstructure, crystallization behaviour and associated magnetic properties of the electroless Ni–Cu–P deposits having various compositions.

2. Experimental procedure

The electroless Ni–Cu–P alloy films were deposited on a 5086 aluminium alloy sheet which had been preplated. The preplating process included cleaning, nitric acid and double zincating treatments. The bath used to obtain the electroless deposits consisted of 21.0–26.3 g dm^{-3} $NiSO_4 \cdot 6H_2O$, 0.0–6.3 g dm^{-3} $CuSO_4 \cdot 5H_2O$, 31.5 g dm^{-3} $NaH_2PO_2 \cdot H_2O$, 58.8 g dm^{-3} sodium citrate and 1.0 p.p.m. thiourea. The ammonia solution was used to adjust the pH of the bath to 9.0. The temperature of the bath was maintained at 80 °C with a thermoregulator and agitated by magnetic stirring.

The P and Cu content in the deposits were analysed by the inductively coupled plasma (ICP) emission spectrometry. The magnetic property of the 1 cm × 1 cm specimens (saturated magnetic moment, M_s) was measured at room temperature in a vibrating sample magnetometer (VSM) with correction made for the Al substrate. The crystallization temperature of the deposits separated from the substrate was measured at heating rate of 10 K min^{-1} by using a ULVAC DSC 7000M.

The separated deposits were also cut to 3 mm diameter discs, both sides of which were thinned by mechanical polishing and further thinned to a suitable thickness for TEM by twin jet polishing. The electrolyte for twin jet polishing consisted of 10% perchloric acid, 10% glycerol and 80% methanol cooled to 0 °C. *In situ* observation of the crystallization process of the deposits was carried out up to 550 °C using furnace-type heating stage with a Jeol EM-SHH heating holder and an EM-SHU2 heater control unit.

Changes in structures of as-deposited and heat-treated films were measured by the usual continuous scanning X-ray diffraction method. However, the interplanar spacing of {1 1 1} planes of the deposits was measured by a step scanning method with a Cu target, in which the step width was 0.05° and the counting

0022–2461/91 $03.00 + .12

time for one step was 100 s. Heat treatment of the deposits used in X-ray diffraction and M_s analyses was carried out isothermally in a salt bath for 2 h at temperatures from 250–450 °C with 50 °C intervals.

3. Results

3.1. Composition

The chemical composition and deposition rate of the electroless Ni–Cu–P deposits obtained from various plating baths are given in Table I. An increase in the $[Cu^{2+}]/[Ni^{2+}]$ ratio in the plating bath resulted in a deposit with higher Cu content and lower P content. The deposition rate increased with increasing $[Cu^{2+}]/[Ni^{2+}]$ ratio up to 0.25, beyond which the deposition rate abruptly decreased and the plating reaction stopped. The decreasing or cessation of the plating reaction was attributed to the abrupt reduction of the catalytic nickel surface by codeposition of Cu atoms on the deposit surface, because Cu is very poor in catalytic activity in hypophosphite bath.

3.2. Magnetic properties

The saturated magnetic moments of heat-treated deposits are shown in Fig. 1. Deposits containing more than about 28.5% Cu content showed stable non-magnetic characteristics even after heating at 400 °C, whereas lower Cu content deposits showed ferromagnetism even after annealing at 300 °C.

3.3. Differential scanning calorimetry (DSC)

All samples but that containing no Cu exhibited more than three reactions including a broad peak ranging from 200–300 °C as can be seen in the exothermic peaks observed below 550 °C in Fig. 2. The temperature and height of the second peak increased and decreased, respectively, with increasing Cu content. The third peak temperatures were nearly constant regardless of Cu content. The DSC results can be explained with reference to the X-ray diffraction and hot-stage TEM analysis results (Figs 3–5) as follows. The first broad peak was caused by coarsening of the pre-existing Ni–Cu solid solution and the second peak could be attributed to transformation of amorphous region into Ni_5P_2 or Ni_5P_2 and Ni_3P phases. The third peak could be ascribed to transformation of the metastable Ni_5P_2 phase into the stable Ni_3P phase.

TABLE I Composition and deposition rate of electroless Ni–Cu–P deposits

$[Cu^{2+}]/[Ni^{2+}]$ (mole ratio)	Composition (wt %)			Deposition rate ($\mu m\ h^{-1}$)
	Ni	Cu	P	
0	89.0	0.0	11.0	10.0
0.05	73.7	15.9	10.4	10.2
0.11	62.7	28.5	8.8	13.0
0.18	48.8	44.5	7.5	13.3
0.25	46.0	50.3	5.7	15.0

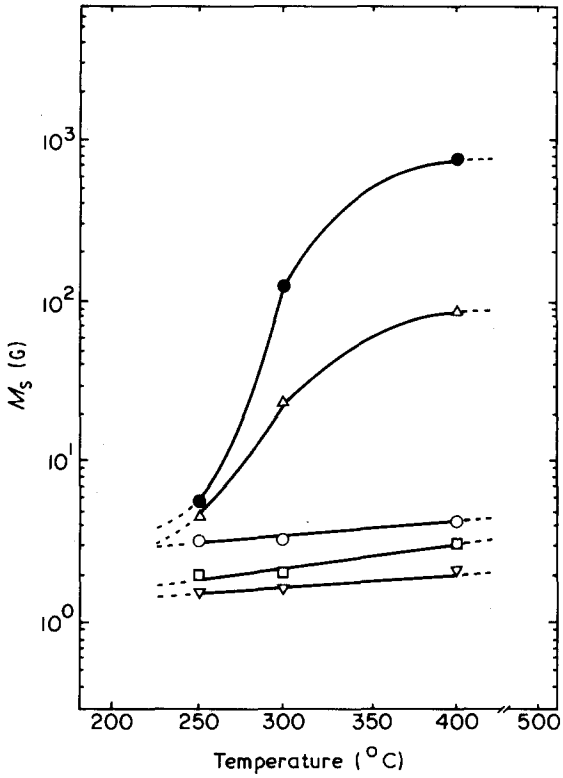

Figure 1 Saturated magnetic moment values of the electroless Ni–Cu–P alloy deposits. Annealing was performed at the various temperatures for 2 h. (●) Ni–11P, (△) Ni–15.9Cu–10.4P, (○) Ni–28.5Cu–8.8P, (▽) Ni–44.5Cu–7.5P, (□) Ni–50.3Cu–5.7P.

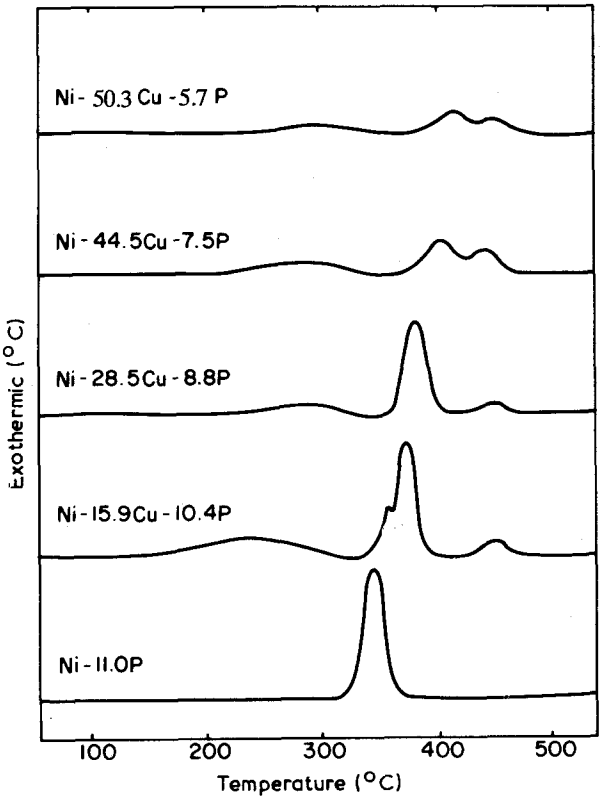

Figure 2 DSC curves of the crystallization process for the electroless Ni–Cu–P alloy deposits.

3.4. X-ray diffraction (XRD) analyses

The X-ray diffraction patterns of deposits annealed at various temperatures are shown in Fig. 3a–e. Considering the (1 1 1) peak position and peak width,

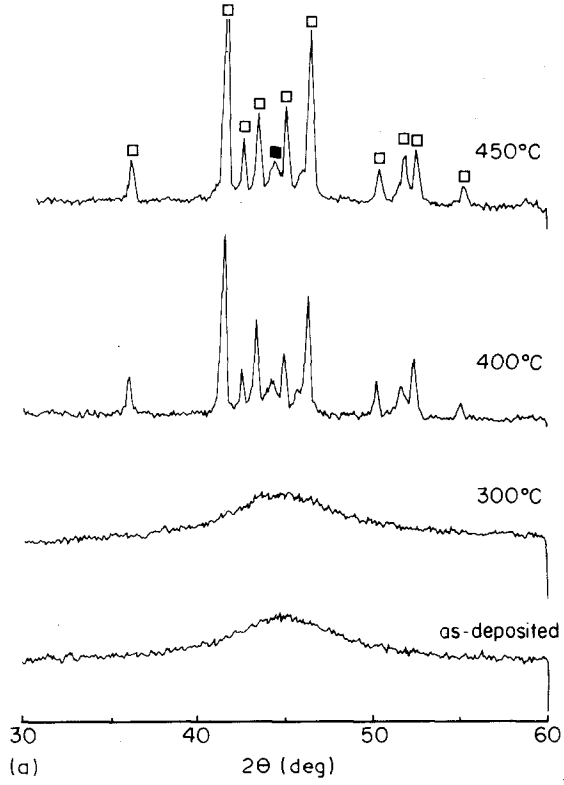

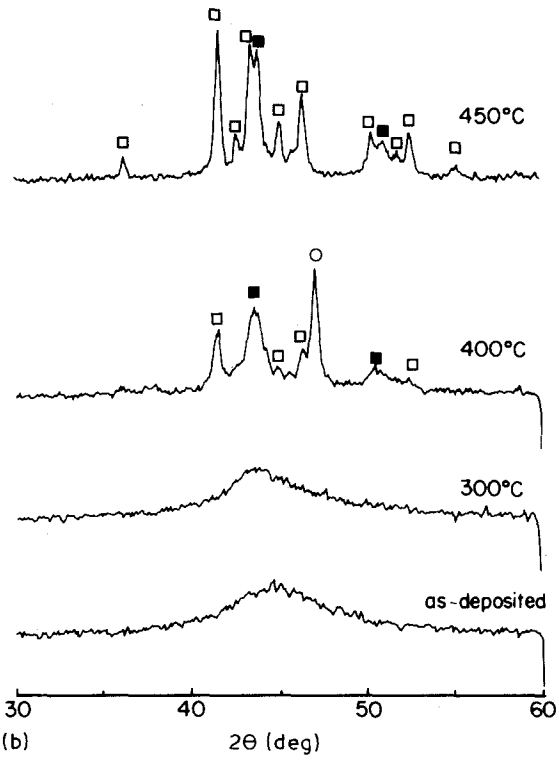

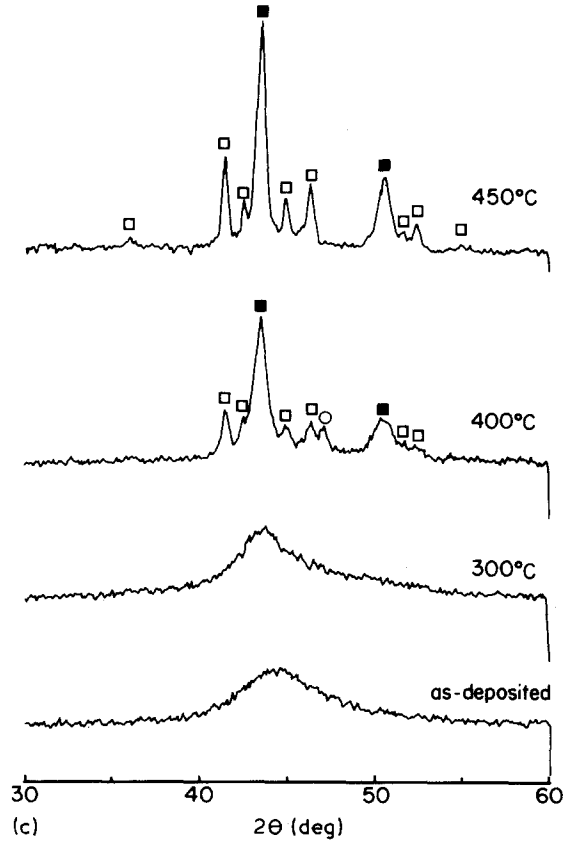

Figure 3 XRD patterns of the Ni–Cu–P alloy deposits. Annealing was performed at the various temperatures for 2 h. (■) Ni–Cu, (□) Ni_3P, (○) Ni_5P_2. (a) Ni–11P, (b) Ni–15.9Cu–10.4P, (c) Ni–28.5Cu –8.8P, (d) Ni–44.5Cu–7.5P, (e) Ni–50.3Cu–5.7P.

the deposits containing high-Cu and low-P [Ni–(44.5–50.3)Cu–(7.5–5.7)P] consisted of microcrystallites of Ni–Cu solid solution, whose crystal size was estimated to be less than 10 nm from the Scherrer formulae and had the [1 1 1] textures, whereas X-ray diffraction patterns of as-deposited samples containing low-Cu and high-P [Ni–(0–28.5)Cu–(11–8.8)P] appeared to indicate amorphous characteristics. The X-ray diffraction pattern of deposits at 300 °C were not very different from that of the as-deposited sample, but the (1 1 1) peak position which shifted towards a low diffraction angle at 400 °C showed simultaneous appearance of peaks of Ni_5P_2 and Ni_3P phases. The X-ray diffraction pattern of the deposit annealed at 450 °C showed only the Ni–Cu solid solution and Ni_3P phase peaks, and the diffraction peaks of Ni_5P_2 were absent. The (1 1 1) peak position of the Ni–Cu solid solution phase shifted further to a lower diffraction angle in the diffraction pattern of the samples annealed at 400 and 450 °C. Cu compounds, such as Cu_3P phase, were not found in all the samples. The interplanar spacing of (1 1 1) planes obtained from the (1 1 1) peak position and the grain size of the Ni–Cu solid solution calculated from the Scherrer formulae are given in Table II. The interplanar spacing increased with increasing copper content and annealing temperature.

3.5. TEM analysis

Fig. 4 shows transmission electron micrographs and diffraction patterns of the Ni–50.3Cu–5.7P alloy films at various heating stages. Under the as-deposited condition, as shown in Fig. 4a–c, crystalline and amorphous areas seem to coexist. The black spots in Fig. 4a seem to be the crystalline region. The diffraction rings in Fig. 4b were indexed as (1 1 1), (2 0 0), (2 2 0) and (3 1 1) planes of an f c c Ni–Cu solid solution and the diffuse haloes accompanied by the rings are ascribed to the amorphous region. The dark-field

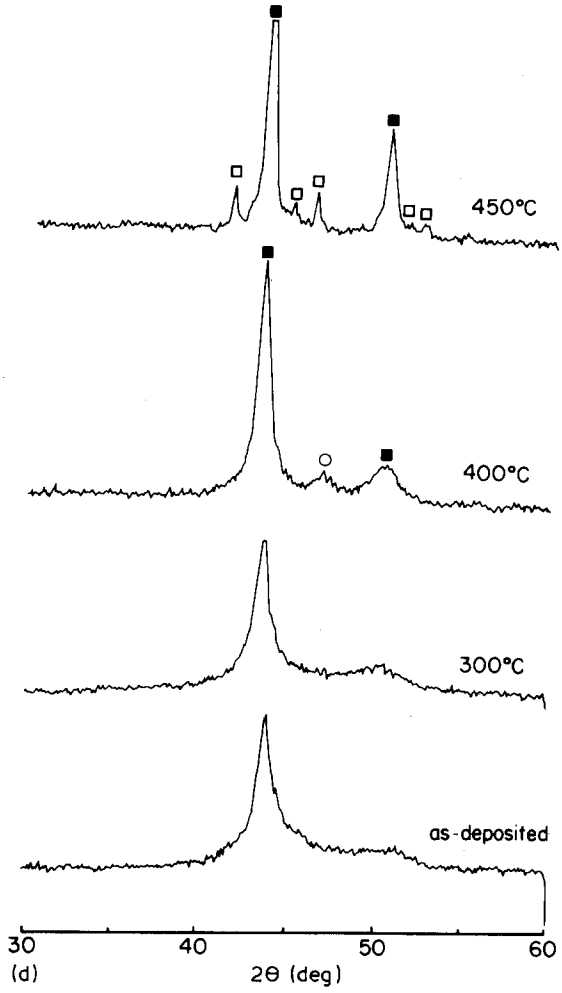

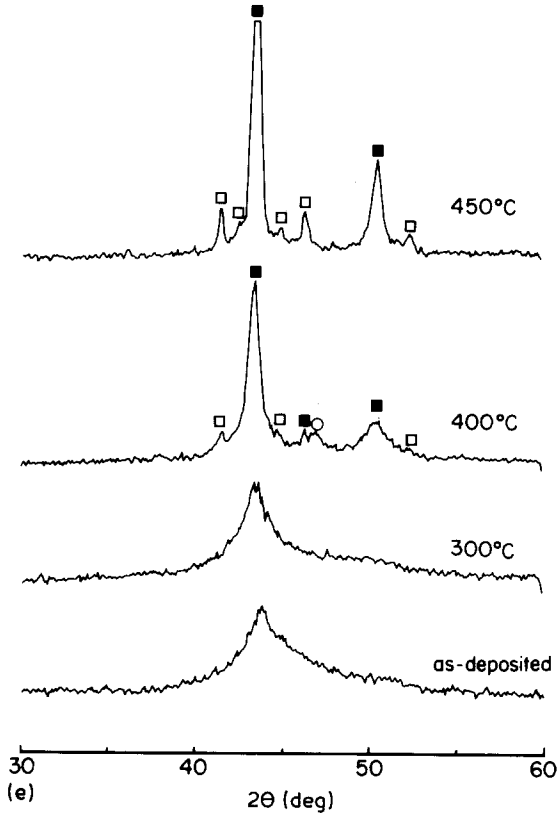

Figure 3 continued

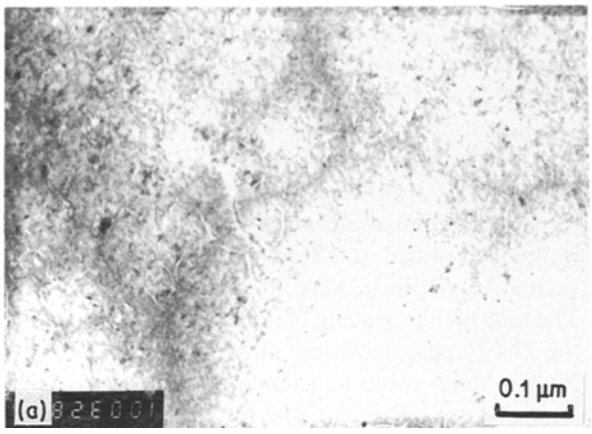

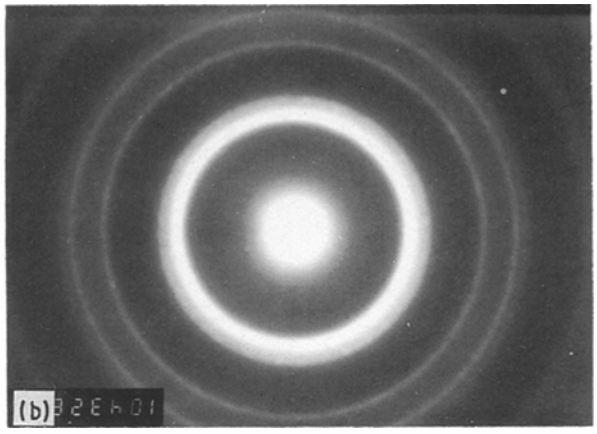

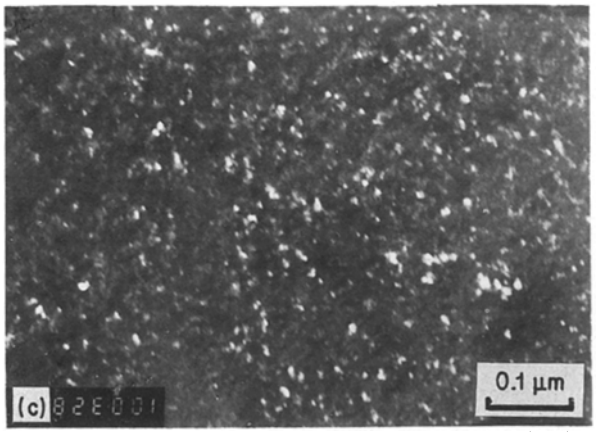

Figure 4 Transmission electron micrographs and electron diffraction patterns of the electroless Ni–50.3Cu–5.7P alloy deposits at various heating stages. (a–c) As-deposited; and heated at (d, e) 380 °C, (f, g) 550 °C; (c) is a dark-field image of (a).

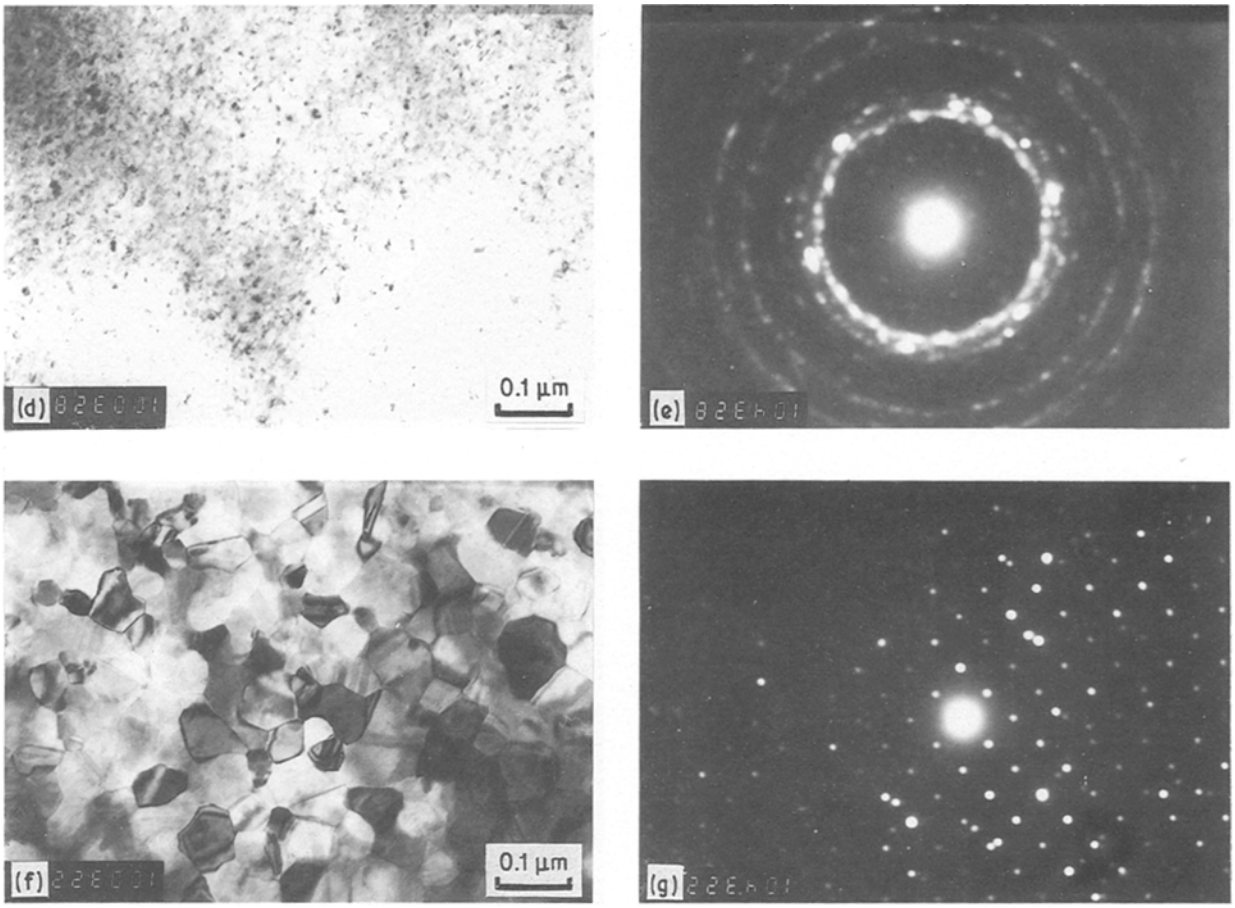

Figure 4 continued

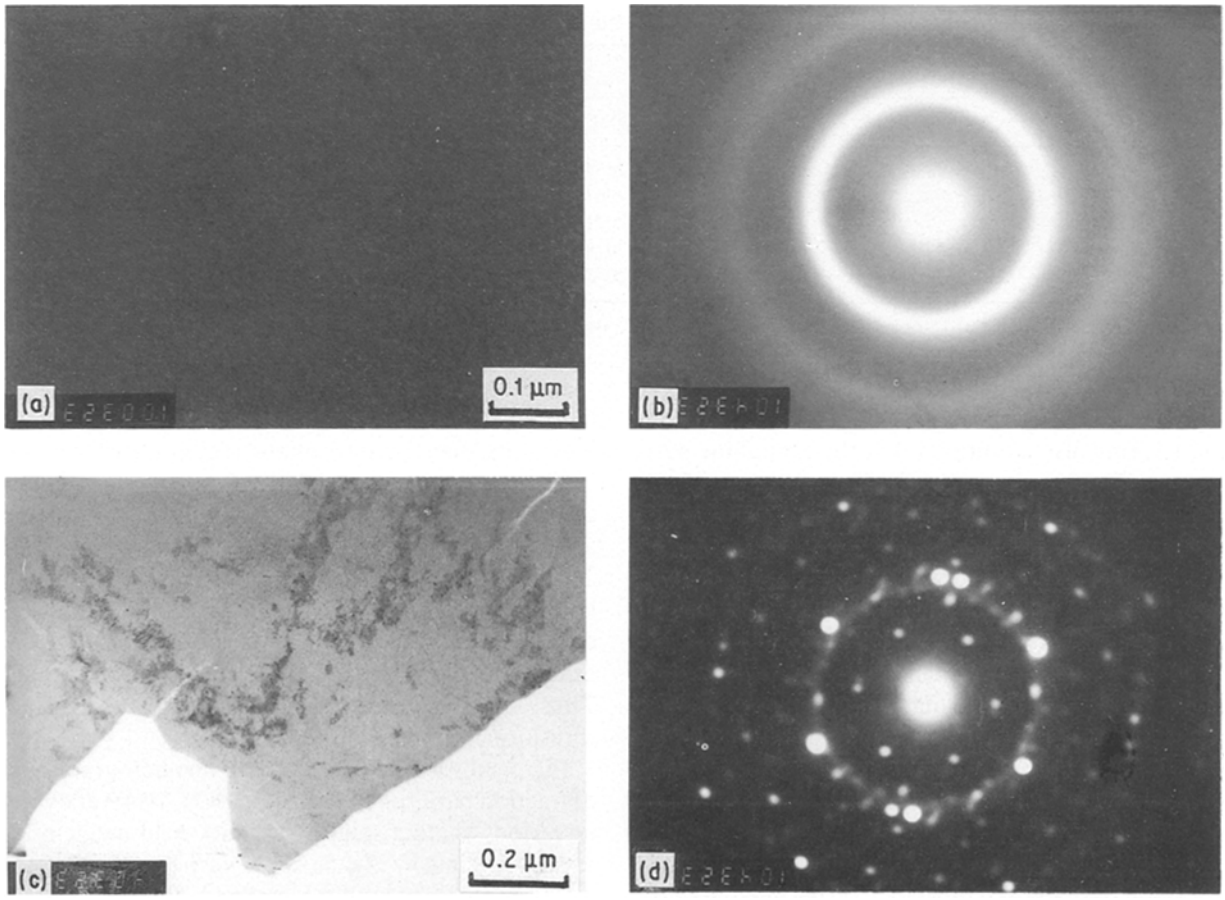

Figure 5 Transmission electron micrographs and electron diffraction patterns of the electroless Ni–15.9Cu–10.4P alloy deposits at various heating stages. (a, b) As-deposited; and heated at (c, d) 350 °C, (e, f) 360 °C, (g) 380 °C, (h) 550 °C.

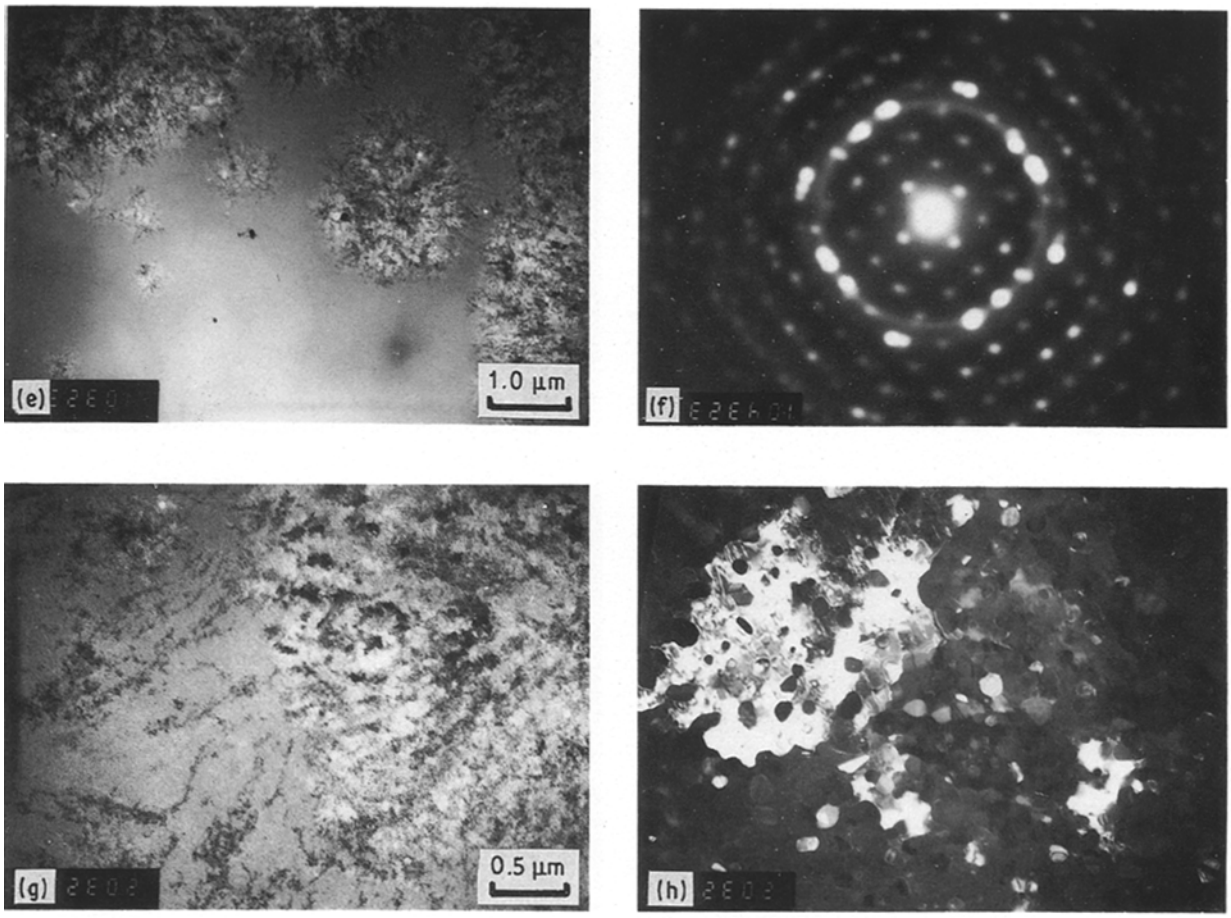

Figure 5 continued

TABLE II Interplanar spacing of (1 1 1) planes and grain size of the Ni–Cu solid solution crystallites in as-deposited and heat-treated films

Alloy	Interplanar spacing (nm) of (1 1 1) plane			Grain size (nm)		
	As-deposited	300 °C	400 °C	As-deposited	300 °C	400 °C
Ni–11.0P	[a]	[a]	0.2034	1.32	1.43	6.13
Ni–15.9Cu–10.4P	[a]	[a]	0.2063	1.43	1.71	10.69
Ni–28.5Cu–8.8P	[a]	0.2063	0.2071	1.79	2.14	8.55
Ni–44.5Cu–7.5P	0.2062	0.2070	0.2078	2.86	3.42	10.69
Ni–50.3Cu–5.7P	0.2063	0.2071	0.2077	6.59	7.13	7.78

[a] The interplanar spacing of {1 1 1} planes was not determined due to its indistinct maximum intensity.

image in Fig. 4c with the objected aperture centred on the (1 1 1) ring also confirmed that the crystalline part was crystalline Ni–Cu solid solution whose grain size was about 10–20 nm. The difference between the grain size calculated from the X-ray diffraction line broadening and the grain size observed from the transmission electron micrograph is thought to be due to residual stresses developed in the specimens during plating, which tend to broaden the diffraction line, and hence the grain size is calculated to be finer than the true size. From the results, it is concluded that as-deposited Ni–50.3Cu–5.7P film consists of Ni–Cu solid solution microcrystallites and amorphous phase.

On heating the Ni–50.3Cu–5.7P film at temperatures below 380 °C, the transmission electron micrographs and diffraction pattern of the specimen did not change, although the microcrystallites slightly coarsened. When heated to 380 °C (Fig. 4d and e), the hexagonal diffraction pattern of Ni_5P_2 was obtained, indicating that the amorphous region transformed to Ni_5P_2 phase and the grain size of the nickel phosphide crystals is large. Fig. 4f and g show the microstructure and diffraction pattern of the film heated at 550 °C. The Ni–Cu solid solution crystallites coarsened to large grains including twins and stacking faults. The diffraction spots were only those of Ni_3P phase and no other phosphide phases were found in that stage. Thus, it is concluded that Ni_5P_2 phase had already transformed into Ni_3P phase.

Fig. 5 shows transmission electron micrographs and diffraction patterns of the Ni–15.9Cu–10.4P alloy film in various heating stages. The dark-field image of as-deposited films in Fig. 5a show very fine Ni–Cu solid solution microcrystallites embedded in amorphous matrix. The diffraction pattern (Fig. 5b) shows only diffuse haloes indicating amorphous characteristics,

due to small quantities and very fine particle sizes of the Ni–Cu solid solution crystallites. On heating the film, the Ni–Cu solid solution crystallites slowly coarsened. At 350 °C, new crystallites, which were indexed as Ni_5P_2, nucleated at the edge of the film and quickly grew into the inner region including the pre-existing Ni–Cu solid solution microcrystallites (Fig. 5c and d). On further heating to 360 °C, Ni_3P crystallites whose microstructures differ from the former, appeared randomly in the inner amorphous matrix (Fig. 5e and f) and grew until they impinged on one another. The microstructure shows spherulitic or dendritic morphology. The spherulitic or dendritic growth resulted in the rejection of the Cu and Ni atoms from the crystallites into the amorphous area ahead of crystallization front. Fig. 5g shows coexisting Ni_5P_2 and Ni_3P phases. On further heating to 380 °C, the Ni_5P_2 phase which nucleated at the edge of the film, transformed into stable Ni_3P phase. A dark-field image of the film at 550 °C (Fig. 5h) shows coarsened Ni–Cu solid solution particles embedded in well-defined large Ni_3P grains. The Ni–50.3Cu–5.7P and Ni–P deposits also showed the same structure as shown in Fig. 5h when heated at 550 °C.

4. Discussion and conclusion

4.1. Magnetization

Non-magnetic amorphous Ni–P deposits turn into ferromagnetic materials when they transform into crystalline nickel and nickel phosphide, Ni_3P and Ni_5P_2. The saturated magnetic moment, M_s, of the Ni–P deposits is mainly proportional to the quantity of the crystalline Ni in them, because Ni_3P phase exhibits a temperature-independent Pauli paramagnetism [9] and the Ni_5P_2 phase is likely to be paramagnetic due to its higher P content. In this study, the Ni–11P amorphous deposits were magnetized at 300 °C. This behaviour is ascribed to pure Ni precipitates embedded in the Ni_3P phase which transformed from the amorphous deposit. All the Ni–Cu–P deposits also showed no ferromagnetism in the as-deposited state regardless of their Cu and P contents even when they were crystallized by heating in the case of higher Cu content.

These results suggest that the Cu content plays a very important role in determining the saturated magnetic moment. According to the band theory, magnetization decreases at a rate proportional to the valence of the solute in Ni-base alloys according to Equation 1 [10]

$$\mu = (0.572 - X)\mu_B \quad (1)$$

where μ, X and μ_B are saturated magnetic moment per atom of Ni–Cu solid solution, atomic fraction of Cu and the Bohr magneton, respectively.

From Equation 1, 57 at % Cu (valence 1) is needed to reduce the magnetic moment of Ni–Cu solid solution to zero. Assuming that there is no P solubility in the crystalline Ni–Cu solid solution and all P in the sample forms Ni_3P, which might be the case for annealed specimens, the saturated magnetic moment of the specimens $[M_s]_{sample}$ can be evaluated from

$$[M_s]_{sample} = [M_s]_{Ni-Cu} f_{Ni-Cu} \quad (2)$$

where $[M_s]_{Ni-Cu}$ and f_{Ni-Cu} are, respectively, saturated magnetic moment (G) and volume fraction of the Ni–Cu solid solution in a sample. $[M_s]_{Ni-Cu}$ may be expressed as

$$[M_s]_{Ni-Cu} = \frac{6084(0.572 - X)v_{Ni}}{0.572[v_{Ni}(1 - X) + v_{Cu}X]} \quad (3)$$

where the quantity 6084 and v_{Ni} are the M_s value (G) and atomic volume of pure Ni and X is the atomic fraction of Cu in an Ni–Cu solid solution. The value of X can be calculated from the measured interplanar spacing of the (1 1 1) plane of the Ni–Cu solid solution using Vegard's law and from the measured Cu concentration of the specimen. The densities of Ni, Cu and Ni_3P used to evaluate the volume fraction of Ni–Cu solid solution and Ni_3P were taken to be 8900, 8960 and 7823 $kg\,m^{-3}$, respectively. The density of the Ni–Cu solid solution was calculated from its atomic volume which was evaluated using Vegard's law.

The calculated results are given in Table III. The calculated saturated magnetic moment of samples annealed at 300 and 400 °C are in reasonably good agreement with the measured data. However, the calculated M_s values for as-deposited samples Ni–44.5Cu–7.5P and Ni–50.3Cu–5.7P, which are more or less crystalline in character, are higher than the measured values. This may be attributed to the fact that the specimens might include some quantity of amorphous phase and/or the Ni–Cu crystallites in

TABLE III Calculated saturated magnetic moments

Annealing temp. (°C)	Alloy	X[a]	Calculated sat. mag. mom. of Ni–Cu crystal (G)	Calculated vol. frac. of Ni–Cu crystal[b]	Calculated sat. mag. mom. of sample (G)
400	Ni–11.0P	0	608	0.240	146
	Ni–15.9Cu–10.4P	0.537	358	0.277	99
	Ni–28.5Cu–8.8P	0.685	0	0.380	0
	Ni–44.5Cu–7.5P	0.815	0	0.465	0
	Ni–50.3Cu–5.7P	0.796	0	0.595	0
300	Ni–44.5Cu–7.5P	0.667	0	0.465	0
	Ni–50.3Cu–5.7P	0.685	0	0.595	0
As-deposited	Ni–44.5Cu–7.5P	0.519	543	0.465	252
	Ni–50.3Cu–5.7P	0.537	358	0.595	213

[a] Measured atomic fraction of Cu.

[b] Calculated assuming that all P forms Ni_3P and the deposits are mixture of Ni_3P and Ni–Cu solid solution crystallites when fully annealed.

them might dissolve P to some degree. It is known [11] that the 3 or 5 outer electrons of the P atom fill the hole in the 3d band of Ni in Ni–P alloys. Assuming that at least 1.0–2.0 at % P was dissolved in the Ni–Cu solid solution crystallites, the measured M_s values are found to be reasonable. For a given chemical composition, the copper content, X, in Ni–Cu solid solutions calculated based on X-ray diffraction results, increased with increasing annealing temperature. This result reflects the fact that P was dissolved in the Ni–Cu crystallites and some Cu was included in the amorphous region in the as-deposited samples, and the P dissolved in the crystallites was being rejected and Cu in the amorphous region was diffusing into crystallites during annealing. The slight increase in M_s values even in the high Cu crystalline specimens with increasing annealing temperature also reflect the solubility of P in the Ni–Cu crystallites in the as-deposited samples.

4.2. Microstructure and crystallization

From the results of the VSM, DSC, X-ray diffraction and TEM analyses, we can see that electroless Ni–Cu–P films consist of fcc Ni–Cu solid solution crystallites and a P-rich amorphous region. The microcrystalline grain size is determined by P content rather than Cu content as in electroless low-P Ni–P alloys [12]. As the P content of the deposits is increased, the growth of the Ni–Cu crystallites becomes difficult, and their grain size becomes finer. The crystallites are Ni–Cu solid solutions dissolving a small amount of P, as discussed in the previous sections.

The crystallization process of the Ni–Cu–P alloys involves at least three stages: (1) pre-existing Ni–Cu solid solution crystallites change into Cu-rich solid solution crystallites by absorbing Cu from the surrounding amorphous phase during coarsening; (2) the Cu-depleted amorphous area crystallizes into Ni_5P_2 or into Ni_5P_2 and Ni_3P; (3) the metastable Ni_5P_2 phase finally transforms into stable Ni_3P phase.

Phase separation into Cu- and Ni-rich phases of Ni–Cu solid solution appearing below 400 °C in the equilibrium phase diagram [13] were not found in this study. If the phase separation occurred, the Ni-rich solid solution would magnetize the deposits and the X-ray diffraction peaks of that phase would appear when annealed.

Acknowledgement

The authors thank the Ministry of Commerce and Industry for financial support of this research.

References

1. A. BRENNER and G. E. RIDDLE, US Pat. 2532283/4 (1950).
2. A. W. GOLDSTEIN, W. ROSTOKER, F. SCHLOSSBERGER and G. GUTZEIT, *J. Electrochem. Soc.* **104** (1957) 104.
3. A. H. GRAHAM, R. W. LINDSAY and H. J. READ, *ibid.* **112** (1965) 401.
4. S. H. PARK and D. N. LEE, *J. Mater. Sci.* **23** (1988) 1643.
5. K. H. HUR, J. H. JEONG and D. N. LEE, *ibid.* **25** (1990) 2573.
6. Y. OKAMURA, S. FUTANI, K. KAWADA, A. KOGA and F. MATSUI, *Kinzoku Hyomen Gijutsu (Jpn)* **38** (1987) 424.
7. K. AOKI, O. TAKANO and S. ISHIBASHI, *ibid.* **30** (1979) 126.
8. M. SAITO and A. NAKABAYASHI, US Pat. 4 724 188 (1988).
9. R. J. GAMBINO, T. R. McGUIRE and Y. NAKAMURA, *J. Appl. Phys.* **38** (1967) 1253.
10. B. D. CULLITY, "Introduction to Magnetic Materials" (Addison-Wesley, Massachusetts, 1972).
11. P. A. ALBERT, Z. KOVAC, H. R. LILIENTAL, T. R. McGUIRE and Y. NAKAMURA, *J. Appl. Phys.* **38** (1967) 1258.
12. R. M. ALLEN and J. B. VANDER SANDE, *Scripta Metall.* **16** (1982) 1161.
13. SRIKANTH and K. J. JACOB, *Mater. Sci. Technol.* **5** (1988) 427.

Received 25 September 1989
and accepted 9 April 1990